*Proceedings of the 21st ICSMGE, Vienna, Austria, 14 – 19 June 2026. Pistrol, Adam & Schweiger (eds.)*
*Published by: ÖGG, Austrian Society for Geomechanics, Salzburg, Austria, ISBN 978-3-9503898-4-5*
*https://doi.org/10.53243/ICSMGE2026-875*

# Laboratory characterisation of the full-strain shearing behaviour of glauconite sand

**Yong Wang,** Tingfa Liu, Erdin Ibraim, Andrea Diambra
*School of Civil, Aerospace, and Design Engineering, University of Bristol, Bristol, UK, yong.wang@bristol.ac.uk*

Mingnan Li, Chris Brandish-Lowe, Toby Masters
*Geoquip Marine, Bristol, UK*

ABSTRACT: Glauconite sand, colloquially known as greensand, is a dioctahedral potassium and iron rich mica and widely found in peloidal form within shallow marine depositional environments in coastal areas. Cone penetration and driven pile installation in glauconite sands are often reported to encounter substantially high resistances, posing significant geotechnical challenges as recognised in earlier construction projects in Antwerp (Belgium) area and recent offshore renewable wind energy development along the Atlantic Outer Continental Shelf. This paper reports outcomes from a preliminary laboratory testing campaign aimed at improving the understanding of the mechanical behaviour of glauconite sand from small-strain range to ultimate failure under monotonic loading conditions. A suite of fully instrumented triaxial tests were performed on reconstituted glauconite sand specimens, supplemented by extensive shear velocity measurements. The results demonstrate how glauconite sand's linear and non-linear small-strain stiffnesses vary systematically with effective stress levels, and how its large-strain and ultimate shearing behaviour may be interpreted within the critical state framework. The outcomes have important applications and implications for advanced modelling and interpretation of the drivability of pile foundations in glauconite sand and their subsequent response to axial and lateral offshore loading.

KEYWORDS: Glauconite sand; undrained shear behaviour; small-strain stiffness; offshore pile foundations.

## 1 INTRODUCTION

The important capabilities and practical values of advanced laboratory testing have been demonstrated in a wide range of geotechnical analysis and design of onshore and offshore infrastructure. Modern design of pile foundations particularly for offshore renewable energy developments demands detailed characterisation of geomaterials' full-strain shearing behaviour from linear elastic range to ultimate failure to enable serviceability (fatigue) and ultimate limit state analysis. Systematic laboratory testing is essential for characterising soil responses (e.g., small-strain stiffness, strength parameters, and large-strain behaviour) and enabling accurate modelling and design for operational and extreme offshore loading (Anderson et al., 2013).

Glauconite sand is often known as "greensand" due to its rich components of glauconite and other minerals. Glauconite sand as an engineering material has posed significant challenges in onshore construction projects in Antwerp area (De Nijs et al., 2015), offshore wind development projects in southern part of the North Sea (Perikleous et al., 2023), and along the northeast coast of the US (Long et al., 2019; Tedrow, 2002; Westgate et al., 2022). High cone resistances and friction ratios were reported in dense sand with high glauconite contents. Recent pile driving practice in North Sea indicated that driven resistances may be underestimated even for sands of lower glauconite content (Perikleous et al., 2023). Site investigation and pile driving in the U.S. Atlantic Outer Continental Shelf area showed significant particle crushing in glauconite sand that led to high soil resistances to driving (SRD) and pile refusal (Pisanò et al., 2025; Westgate et al., 2024).

This experimental study complements earlier extensive research into glauconite sand's index properties (Westgate et al., 2025; Zeppilli et al., 2024), shear strength (Konstantinou et al., 2025; Westgate et al., 2023; Zou et al., 2025), compressibility (Peralta et al., 2025) and interface shearing behaviour (Quinteros et al., 2023), focusing on its small-strain stiffness and ultimate shear failure behaviour. Preliminary outcomes from a series of instrumented undrained triaxial tests are presented with detailed interpretation of the material's full-strain shearing behaviour under monotonic loading.

## 2 MATERIAL, APPARATUS AND PROGRAMME

The glauconite sand employed in this study was retrieved from the Atlantic Outer Continental Shelf area. The as-received bulk samples were well preserved in sealed bags prior to laboratory testing to avoid significant changes in water content. The particle size distribution (PSD) curve as shown in Figure 1 was obtained through a combined wet sieving and hydrometer analysis method that applied a standard four hour shaking of sand and sodium hexametaphosphate (SHMP) solution mixtures (BSI, 2016). Atterberg limits were determined using the fall-cone and thread-rolling methods following the BSI (2018) guidance. The specific gravity ($G_s$) was determined using small pycnometer on moist and oven-dried materials, in accordance with BS EN ISO 17892-3 (BSI, 2015). Table 1 summarises the key particle size characteristics and index properties. The initial water content of the 'as-received' material was ≈20%, close to its plastic limit.

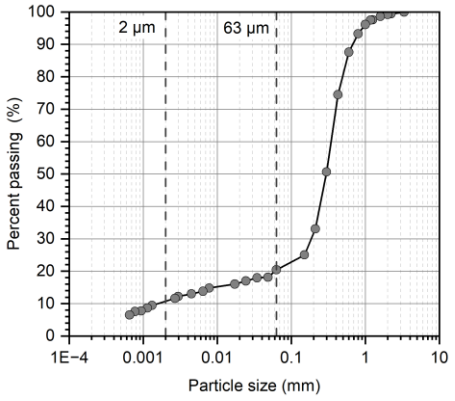


Figure 1. Particle size distribution of the glauconite sand used in this study.

A GDS advanced dynamic triaxial testing system (DYNTTS) testing samples of 50 mm in diameter and 100 mm in height was used in this study. The system is fully instrumented with multi-axis bender elements (BE) that enable non-destructive measurements of P and S wave velocities, as

well as high resolution local axial and belt-type radial Linear Variable Differential Transformer (LVDTs). Feng et al. (2025) report in a parallel study how the triaxial system was used to investigate the primary wave velocities and constrained moduli of a dry glauconite sand. Sintered bronze porous stone disks with smooth surfaces were used to mitigate constraints at specimen ends.

Reconstituted specimens were prepared using the moist tamping method at the 'as-received' water content, following the ASTM D4767-11 method (ASTM, 2020). Target dry densities were achieved by compacting the materials in six layers. Relatively high back pressures of 700-800 kPa were applied to specimens to obtain full saturation with 0.96 or higher Skempton B values. Isotropic consolidation was applied at a rate of 1 kPa/min to achieve target initial mean effective stress ($p_0'$). Drained creep stages of at least 48 hours were applied until the residual local axial strain rates fell below 0.02 %/day. Finally, undrained shearing was applied at a strain rate of 0.01 mm/min (14.4 %/day). Post-test water content and mass measurements were undertaken to double check the specimen's initial dry mass and water content. The specimens' initial conditions and void ratios are summarised in Table 2. The numbers given in the sample ID, for example 400-1.70, represent the initial effective confining pressure (400 kPa) and target dry density (1.70 g/cm$^3$), respectively. The number in the bracket indicates the value of OCR.

Table 1. PSD characteristics and index properties of glauconite sand.

| Parameter | value |
|---|---|
| $D_{10}$ (mm) | 0.002 |
| $D_{30}$ (mm) | 0.198 |
| $D_{50}$ (mm) | 0.297 |
| $D_{60}$ (mm) | 0.346 |
| Fines content, FC (%) | 20.5 |
| Specific gravity, $G_s$ | 2.88 |
| Liquid limit, $w_L$ (%) | 53.9 |
| Plastic limit, $w_P$ (%) | 20.5 |
| Plasticity Index, $I_P$ (%) | 33.4 |

Table 2. Triaxial compression test programme on glauconite sand.

| Sample ID | Target dry density, $\rho_d$ (g/cm$^3$) | Initial void ratio, $e_0$ | Void ratio prior to shearing, $e_c$ | OCR |
|---|---|---|---|---|
| CIU100-1.50 | 1.50 | 0.894 | 0.845 | |
| CIU100-1.70 | 1.70 | 0.749 | 0.719 | |
| CIU200-1.70 | 1.70 | 0.739 | 0.678 | 1 |
| CIU400-1.70 | 1.70 | 0.739 | 0.655 | |
| CIU800-1.70 | 1.70 | 0.749 | 0.596 | |
| CIU200(4)-1.70 | 1.70 | 0.736 | 0.630 | 4 |

## 3 RESULTS AND DISCUSSION

### 3.1 *Isotropic compression response*

The variations of specific volume ($v$) measured from local strain sensors against effective pressure ($p'$) during isotropic consolidation are plotted in Figure 2. All specimens exhibited clear compressive volume changes that increased with the effective stresses. Substantial creep straining can be observed as the specimens were left under maintained constant effective stress conditions for extended periods. Earlier studies by Liu (2018), among others, on silica sands demonstrated how the materials' monotonic and cyclic triaxial shearing behaviour may be affected by any residual creep straining. No clear yielding can be observed within the applied $p'$ range up to 800 kPa. Wang (2025) reported parallel high pressure ($\sigma_v$ up to 76 MPa) constant rate compression (CSR) tests on the same glauconite sand material and identified 1-D yield stresses of 800-1000 kPa that varied marginally with applied compression rates.

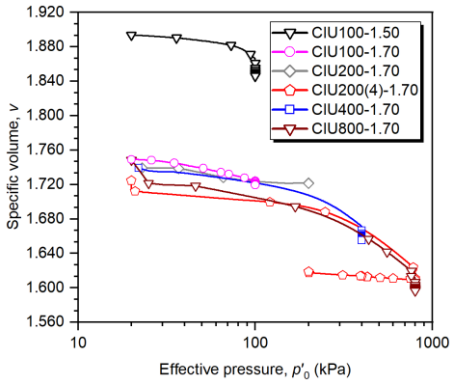


Figure 2. Specific volume change against effective pressure during isotropic consolidation.

### 3.2 *Undrained shearing behaviour*

Figure 3 summarises the key outcomes of the material's undrained shearing response. Area and membrane constraint corrections (Hellings, 1989) were applied to the large axial strain shearing data. The stress-strain responses shown in Figure 3(a) exhibit peak strengths after initial 1-2% axial strain shearing, followed by decreasing strengths that did not recover as shearing continued. Stable excess water pressure trends are plotted in Figure 3(b). The over-consolidated specimen (OCR = 4) tested under $p_0'$ = 200 kPa developed substantially higher strengths and negative excess pore pressures with increasing strain, compared with its counterpart specimen (OCR = 1), reflecting clear effects of increased density and effective stress history.

The normalised stress ratios ($q/p'$) plotted in Figure 3(c) show consistently decreasing post-peak trends that do not seem to converge fully at ultimate states. The higher $p_0'$ tests appear to develop lower ultimate stress ratios of ≈0.70 ($\varphi'_{ult} \approx 18.2°$), in contrast with the lower $p_0'$ tests. Close inspection of the specimens during shearing indicated mostly parabolic deformation without development of clear shear bands. The effective stress paths of all specimens are presented in Figure 3(d), including the OCR = 4 specimen that showed clear tendency to dilate. Also plotted is the interpreted Mohr-Coulomb effective strength envelope with average peak stress ratio $M$ of 0.98 and $\varphi'_{peak} = 25.1°$. The overall shearing response may be interpreted within the critical state framework.

The peak and ultimate state strength parameters are summarised in Table 3. The $\varphi'_{peak}$ values obtained for the tested glauconite sand fall within the value ranges reported by Westgate et al. (2023) of 22-31° and by Zou et al. (2025) of 23-30°, noting the potential effects of material index and mineralogical properties, shearing stress paths and other factors.

Table 3. Summary of stress ratio and strength parameters.

| Sample ID | $p'_0$ (kPa) | $q/p'_{peak}$ | $\varphi'_{peak}$ (°) | $q/p'_{ult}$ | $\varphi'_{ult}$ (°) |
|---|---|---|---|---|---|
| CIU100-1.50 | 100 | 0.89 | 22.9 | 0.86 | 22.2 |
| CIU100-1.70 | 100 | 1.03 | 26.1 | 0.86 | 22.1 |
| CIU200-1.70 | 200 | 0.94 | 23.9 | 0.86 | 22.1 |
| CIU200(4)-1.70 | 200 | 1.00 | 25.4 | 0.74 | 19.3 |
| CIU400-1.70 | 400 | 1.03 | 26.2 | 0.73 | 19.1 |
| CIU800-1.70 | 800 | 1.03 | 26.1 | 0.70 | 18.2 |

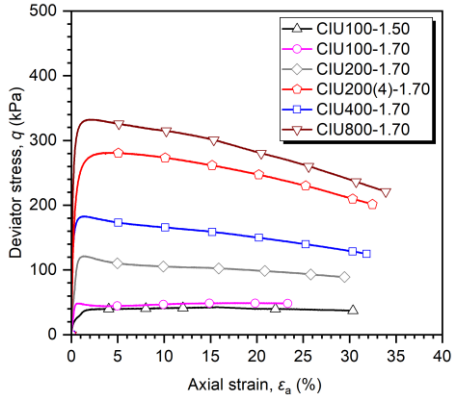


(a)

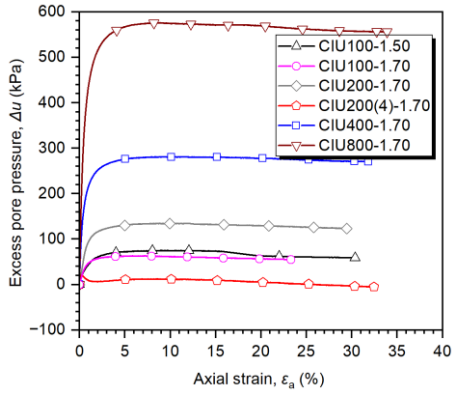


(b)

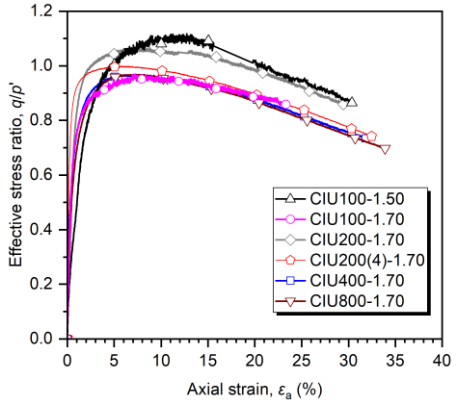


(c)

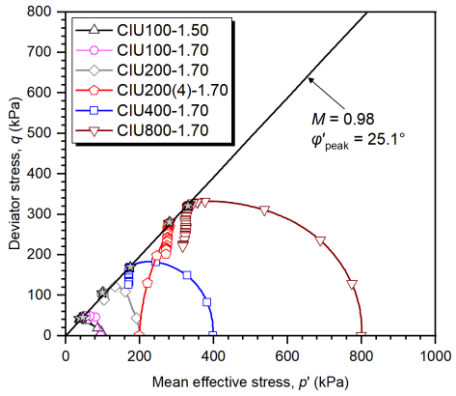


(d)

Figure 3. Consolidated undrained triaxial compression shearing response of glauconite sand: (a) stress-strain behaviour; (b) excess pore water pressure development; (c) stress ratio against axial strain; (d) effective stress paths.

### 3.3 *Small-strain stiffness*

Linear elastic shear stiffnesses ($G_{vh}$) of the glauconite sand were characterised by BE tests performed after full consolidation and creep. The maximum undrained Young's moduli ($E_u^{max}$) were interpreted from very small strain (local $\varepsilon_a$ <0.001%) data through linear regression (Liu, 2018). Figure 4 shows the normalised $G_{vh}$ and $E_u^{max}$ values by a void ratio function $f(e) = (2.17\text{-}e)^2/(1+e)$ (Hardin & Richart, 1963) against effective stress $p'$. Data for some tests were not available due to lack of BE measurements or malfunctioning LVDTs. Tentative power-law functions ($G_{vh}/f(e)=A(p')^n$) are fitted to the $G_{vh}$ data, distinguishing the normally consolidated and over-consolidated specimens, with the latter exhibiting higher constant $A$ but lower exponent $n$. Similar interpretation can be applied to the available $E_u^{max}$ data. A broad $E_u^{max}/G_{vh}$ ratio of ≈3 expected for isotropic soil media can be observed, although the effect of over-consolidation appears less discernible on Young's moduli.

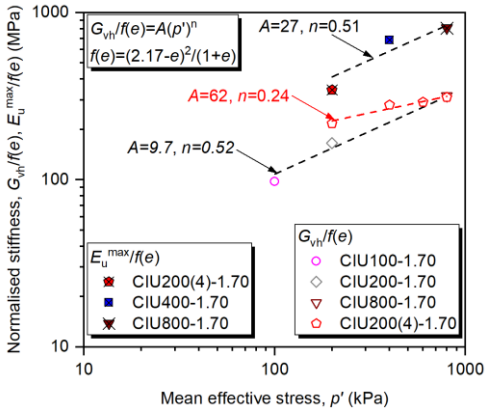


Figure 4. Variation of normalised shear stiffness ($G_{vh}$) and maximum undrained Young's moduli ($E_u^{max}$) against effective stress.

Figure 5 shows an example of the degradation trend of normalised secant undrained Young's modulus ($E_u^{sec}/3$) and the shear stiffness ($G_{vh}$) measured during small strain shearing in test CIU800-1.70. In contrast with the 'static' moduli measured from local strain sensors, the 'dynamic' shear stiffnesses from BE show modest degradation with increasing axial strain levels. These outcomes align with observations from experiments by Liu (2018) and discrete element modelling (DEM) by Li et al. (2022).

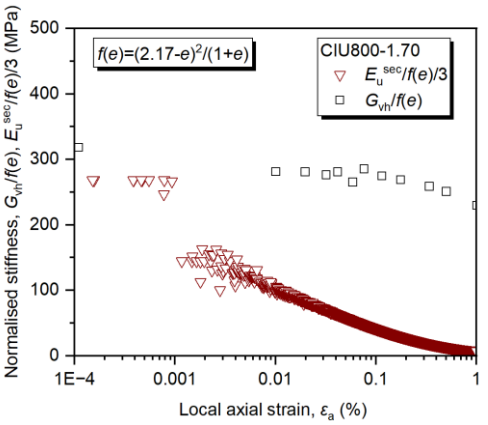


Figure 5. Degradation of normalised shear stiffness ($G_{vh}$) and secant modulus ($E_u^{sec}/3$) against local axial strain for test CIU800-1.70.

## 4 CONCLUSIONS

Glauconite sand pose significant engineering challenges for a wide range of onshore and offshore infrastructure projects. This paper reports outcomes from a preliminary triaxial testing programme on glauconite sand that focused on its full-strain shearing behaviour from linear elastic small strain range to large-strain ultimate failure. Key conclusions drawn from the study are summarised as follows:

(1) The tested glauconite sand contained high amount of plastic fines and developed significant creep deformation under maintained stress conditions.

(2) The normally consolidated glauconite specimens developed peak strengths at early shearing strains, followed by decreasing trends as shearing continued to ultimate states. In contrast, the over-consolidated specimen developed substantially higher strengths and significant dilation. The overall shearing response can be interpreted within the critical state framework.

(3) The material's shearing resistance angles appear to fall within the value ranges reported for glauconitic sands found in Coastal Plain of New Jersey and the Atlantic Outer Continental Shelf area.

(4) Combined bender element and local strain measurements enabled detailed characterisation of the material's linear elastic stiffnesses. Power-law functions may be introduced to fit the normalised stiffness against effective stress trends. The over-consolidation history appears to have major impact on shear stiffness but relatively minor influence on Young's modulus.

(5) Different degradation patterns were observed between 'static' moduli measured from local strain sensors and 'dynamic' shear stiffnesses obtained from bender elements. The latter exhibited modest degradation with increasing strain levels.

## 5 ACKNOWLEDGEMENTS

This study was undertaken as part of a Strategic Partnership between the University of Bristol and Geoquip Marine. The first Author thanks the joint financial support by Engineering and Physical Science Research Council (EPSRC, EP/W524414/1) and Geoquip Marine for his doctoral research. GDS Instruments is thanked gratefully for the additional financial and technical support for the advanced cyclic triaxial equipment employed in the study. Useful discussions with Mr. Gary Martin, Dr. Borui Ge and Mr. Zhixin Zhou of the University of Bristol, and Daniel Smith, Peter Webster and Dariusz Guzik of Geoquip Marine are also acknowledged.

## 6 REFERENCES

Andersen, K. H., Puech, A. A., & Jardine, R. J. (2013). Cyclic resistant geotechnical design and parameter selection for offshore engineering and other applications. *Proceedings of ISSMGE - TC 209*(14), 12.

ASTM. (2020). *D4767-11(2020) Standard Test Method for Consolidated Undrained Triaxial Compression Test for Cohesive Soils*. West Conshohocken, PA: ASTM International.

BSI. (2015). *BS EN ISO 17892-3-2015-Geotechnical investigation and testing laboratory testing of soils. Part 3: Determination of particle density*. London, UK: British Standards Institution.

BSI. (2016). *BS EN ISO 17892-4-2016- Geotechnical investigation and testing — Laboratory testing of soil Part 4: Determination of particle size distribution*. London, UK: British Standard Institution.

BSI. (2018). *BS EN ISO 17892-12-2018+A2-2022-Geotechnical investigation and testing. Laboratory testing of soil. Determination of liquid and plastic limits*. London, UK: British Standard Instituion.

De Nijs, R., Kaalberg, F., Osselaer, G., Couck, J. v., & Van Royen, K. (2015). Full-scale field test (sheet) pile drivability in Antwerp (Belgium). *Geotechnical Engineering for Infrastructure and Development*.

Feng, S., Li, M., Reyhanianasl, P., Brandish-Lowe, C., Masters, T., Ibraim, E., Liu, T. & Diambra, A. Laboratory investigation of primary wave velocities and constrained moduli of glauconite sand under anisotropic stress states. In *ICSMGE Vienna 2026*.

Hardin, B. O., & Richart Jr, F. (1963). Elastic wave velocities in granular soils. *Journal of the soil mechanics and foundations division*, 89(1), 33-65.

Hellings, J. E. (1989). *The strength and stiffness of soils associated with excavations.* PhD thesis. University of London, London, UK.

Konstantinou, M., Piedrabuena, A. R., Hellebrekers, N., Mento, M., Elkadi, A. S. K., & Gavin, K. G. (2025). Geotechnical Properties of a Glauconite Sand from Belgium. *5th International Symposium on Frontiers in Offshore Geotechnics*, Nantes, France.

Li, Y., Otsubo, M., & Kuwano, R. (2022). Interpretation of static and dynamic Young's moduli and Poisson's ratio of granular assemblies under shearing. *Computers and Geotechnics*, *142*, 104560.

Liu, T. (2018). *Advanced laboratory testing for offshore pile foundations under monotonic and cyclic loading*. PhD thesis. Imperial College London. London, UK.

Long, X., Tucker, G., Gibbs, P., Westgate, Z., Diaz, A. T., & Senanayake, A. (2019). Soil classification and evaluation of preconsolidation stress of Atlantic Outer Continental Shelf OCS sediments from oedometer and cone penetration testing. *Offshore Technology Conference*.

Peralta, P., Vembu, K., & Esmailzadeh, S. (2025). The yield strength and compressibility of glauconitic sands in the US Atlantic Outer Continental Shelf. *5th International Symposium on Frontiers in Offshore Geotechnics*, Nantes, France.

Perikleous, G., Meissl, S., Diaz, A., Stergiou, T., & Ridgway-Hill, A. (2023). Monopile installation in glauconitic sands. *SUT Offshore Site Investigation and Geotechnics*.

Pisanò, F., Westgate, Z., Rahim, A., Maldonado, C., Komurka, V., Beemer, R., Stuyts, B., Hamre, L., Eiksund, G., & Liedtke, E. (2025). The Piling in Glauconitic Sand (PIGS) JIP: insights from axial and lateral pile load testing. *5th International Symposium on Frontiers in Offshore Geotechnics*, Nantes, France.

Tedrow, J. C. (2002). Greensand and greensand soils of New Jersey: a review. *Rutgers Cooperative Extension*, NJ Agricultural Experiment Station, Rutgers.

Quinteros, V., Westgate, Z., Vinck, K., Dantal, V., Lindtorp, A., & Toma, M. (2023). Interface friction angle of glauconitic sands for pile design. *Offshore Site Investigation Geotechnics 9th International Conference Proceeding*,

Wang, Y. (2025). *One-dimensional consolidation behaviour of glauconite sands under constant rate of strain loading*. MSc Dissertation. University of Bristol.

Westgate, Z., DeGroot, D., Zhang, G., Beemer, R., Miller, K., Browning, J., Coffman, R. A., Senanayake, A., & Maldonado, C. (2025). Piling in Glauconitic Sand (PIGS) JIP: Insights from site characterisation and laboratory testing. *5th International Symposium on Frontiers in Offshore Geotechnics*, Nantes, France.

Westgate, Z., McMullin, C., & DeGroot, D. (2022). Glauconite Sand Challenges for US Offshore Wind Development. *International Conference on Offshore Mechanics and Arctic Engineering*.

Westgate, Z., Rahim, A., Senanayake, A., Pisanò, F., Maldonado, C., Ridgway-Hill, A., Perikleous, Y., De Sordi, J., Roux, A., & Andrews, E. (2024). The Piling in Glauconitic Sands (PIGS) JIP: Reducing Geotechnical Uncertainty for US Offshore Wind Development. *Offshore Technology Conference*.

Westgate, Z. J., DeGroot, D. J., McMullin, C., Zou, Y., Guo, D., Van Haren, S., Beemer, R. D., Zeppilli, D., Miller, K. G., & Browning, J. V. (2023). Effect of degradation on geotechnical behavior of glauconite sands from the U.S. Mid-Atlantic Coastal Plain. *Ocean Engineering*, 283, 115081.

Zeppilli, D., Dennis, E., Westgate, Z., Zhang, G., DeGroot, D., Miller, K., Browning, J., & Beemer, R. (2024). Atterberg Limits of Two Crushed and Natural Glauconite Soils. *Geo-Congress 2024*.

Zou, Y., DeGroot, D. J., & Westgate, Z. J. (2025). Direct and Interface Shear Behavior of an Authigenic Glauconite Sand from the Coastal Plain of New Jersey. *Journal of Geotechnical and Geoenvironmental Engineering*, 151(7), 04025065.